The Miniature Atomic Clock – Pre-Production Results

R. Lutwak and A. Rashed
Symmetricom - Technology Realization Center
Beverly, MA
U.S.A.
RLutwak@Symmetricom.com

M. Varghese, G. Tepolt, J. Leblanc, and M. Mescher
Charles Stark Draper Laboratory
Cambridge, MA
U.S.A.

D.K. Serkland and G.M. Peake
Sandia National Laboratories†
Albuquerque, NM
U.S.A.

***Abstract*— The authors have developed a Miniature Atomic Clock (MAC) for applications requiring atomic timing accuracy in portable battery-powered applications. Recently, we have completed a pre-production build of 10 devices in order to evaluate unit-to-unit performance variations and to gain statistical confidence in the performance specifications, environmental sensitivity, and manufacturability.**

I. INTRODUCTION

Atomic clocks play an essential role in the precise timing and synchronization of modern communications and navigation systems. To date, the relatively large size and power consumption of existing technologies have prevented the deployment of atomic clocks in portable, battery-powered applications. However, the demand for high precision timing in portable devices is steadily increasing for applications in broadband and secure communications and precise location and navigation systems.

Since 2002, the authors have been developing a Chip-Scale Atomic Clock (CSAC), with an emphasis on small size, low-power, and batch fabrication techniques for lower cost. At the 2005 *Frequency Control Symposium*, we reported on the demonstration of a prototype Miniature Atomic Clock (MAC), with an overall size of 10 cm^3, power consumption <200 mW and short-term stability, $\sigma_y(\tau) < 1\times10^{-9}\tau^{-1/2}$ [1]. The reader is referred to that paper for additional references, which describe in detail the fundamental research and design tradeoffs which underlie the evolution of the current design.

Since our previous report, we have continued the development of the prototype MAC to improve performance, usability, and manufacturability. In particular, the short-term stability has been improved by a factor of two, the power consumption has been reduced to 125 mW, and the microwave synthesizer has been redesigned to allow for a precise calibrated output at 10.0 MHz. The firmware has evolved to provide for autonomous acquisition and operation, internal state-of-health determination, and remote calibration and status monitoring.

In this paper, we review the MAC architecture, with particular attention to those aspects which have changed since our previous report, as well as the results of testing of 10 prototype MACs, including short-term stability, frequency drift, temperature coefficient, and power-on retrace.

II. THE MINIATURE ATOMIC CLOCK

A. Architecture

In order to achieve compact size and low-power operation, the MAC physics package interrogates the cesium hyperfine resonance with the technique of Coherent Population Trapping (CPT) rather than the microwave double-resonance scheme employed in conventional vapor-cell atomic clocks[2,3,4]. Interrogation of the CPT resonance is accomplished by the application of a coherently bichromatic optical field, near to the cesium "D1" transition at 894 nm, which is produced by modulating the bias current of a high-bandwidth Vertical-Cavity Surface Emitting Laser (VCSEL) at one-half of the ground state hyperfine frequency, $\nu_0/2 \approx 4.6$ GHz. The advantages of this interrogation scheme include the elimination of the high-power RF discharge lamp and tuned microwave cavity of the conventional design.

The choice of cesium over rubidium is dictated by the higher vapor density of cesium, which leads to lower operating power, and by the superior reliability of VCSELs at cesium wavelengths.

B. Physics Package

The MAC physics package is shown below in Figure 1.

†Sandia is a multiprogram laboratory operated by Sandia Corporation, a Lockheed Martin Company, for the United States Department of Energy's National Nuclear Security Administration under contract DE-AC04-94AL85000.
This work is supported by the Defense Advanced Research Products Agency, Contract # NBCHC020050.
Approved for Public Release, Distribution Unlimited

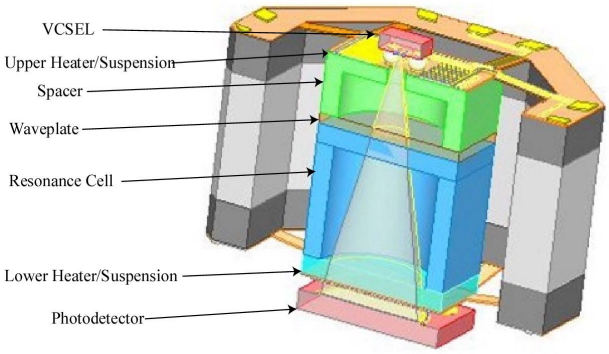

Figure 1. Second-generation Physics package

The second-generation physics package includes the major elements of the successful prototype design described previously with several improvements which enhance its performance and manufacturability[5,6].

The essential elements of the physics package are the resonance cell, shown in blue, and the VCSEL and photodetector, located above and below the resonance cell respectively. The resonance cell is comprised of a silicon body 2 mm square and 2 mm thick with anodically-bonded transparent Pyrex® windows, following the technique pioneered by Liew [7]. The sealed cell contains a small amount of metallic cesium as well as a temperature-compensating mixture of buffer gases. The VCSEL is mounted on the upper suspension, which is spaced from the cell in order to allow divergence prior to the cell in order to reduce the inhomogeneous light shift and effectively illuminate the cell volume. A custom low-threshold high-bandwidth VCSEL, operating at the cesium D1 wavelength of λ=894.3 nm was developed specifically for this application[8]. The choice of the D1 wavelength rather than the more readily available D2 wavelength (λ=852.4 nm) is dictated by the superior CPT signal quality at the D1 wavelength [9,10]. Immediately prior to entering the resonance cell, the VCSEL beam passes through a quarter-wave retarder, oriented with its principal axis at 45° to the laser polarization in order to generate a circularly-polarized field in the interaction volume.

The physics assembly is temperature stabilized at ≈85°C in order to generate sufficient cesium vapor pressure and to stabilize the wavelength of the VCSEL. The power constraints of the MAC thus demand a high degree of thermal isolation between the physics package and the ambient thermal environment. Vacuum-sealing the entire physics assembly eliminates the predominant mode of thermal loss, which is conduction and convection through the gaseous ambient. The cell is suspended, above and below, by a pair of strained polyimide suspensions, which provide both thermal isolation and mechanical support. Resistive platinum heaters, as well as the electrical connections to the optoelectronic components, are patterned onto the polyimide, which permits their mechanical dimensions, and thus their thermal conductivity, to be determined by electrical, rather than mechanical, requirements. The dominant heat loss mechanism from the physics assembly is thus thermal radiation from the heated area to the surrounding package.

In normal operation, the physics package is heated to ≈85°C in a 25°C ambient, requiring approximately 10 mW of heater power. The temperature, VCSEL bias current, and microwave power are then adjusted to optimize the CPT resonance signal as shown below in Figure 2.

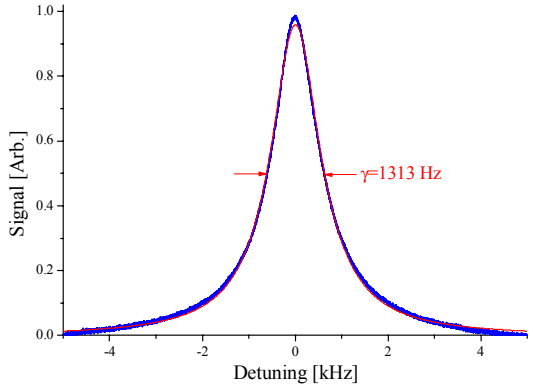

Figure 2: CPT resonance. Red – data, Blue – Lorentzian fit

The linewidth of the CPT resonance is $\gamma \approx 1300$ Hz and the contrast (measured as CPT amplitude divided by the DC light level) is typically ≈ 1%.

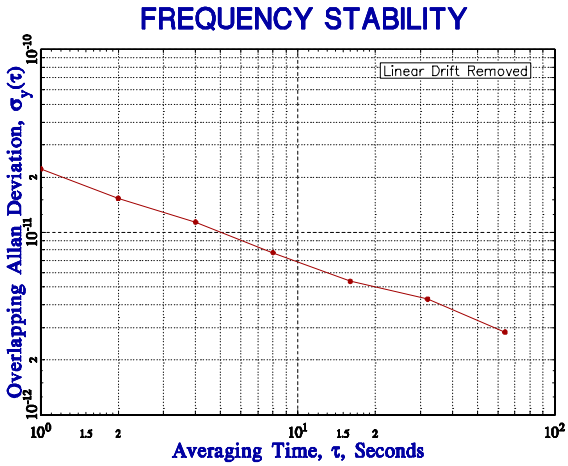

Figure 3. MAC physics package frequency stability

Figure 3 shows typical short-term frequency stability of a MAC physics package, measured with optimal laboratory-scale electronics. All 10 of the physics packages built for the MAC prototypes have demonstrated short-term stability, measured in this optimal fashion, of $\sigma_y(\tau) < 1 \times 10^{-10}\, \tau^{-1/2}$, with most falling into the range of $\sigma_y(\tau) = 2\text{-}4 \times 10^{-11}\, \tau^{-1/2}$.

C. *Microwave Synthesis*

The functional purpose of the MAC microwave synthesizer is to simultaneously provide a spectrally pure clock output at 10.0 MHz along with a coherently synthesized tunable source at 4.596 GHz for the atomic interrogation. Figure 4 shows a block diagram for the MAC microwave synthesizer.

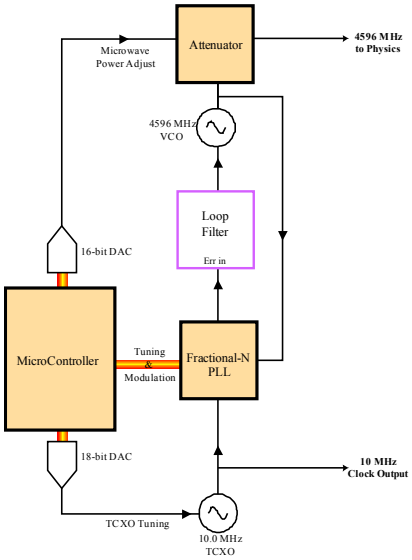

Figure 4. Microwave Synthesizer

The microwave synthesizer consists of a 4596 MHz voltage-controlled oscillator (VCO), which is phase-locked to a 10 MHz temperature-compensated crystal oscillator (TCXO) via a low-power fractional-N phase-locked loop (PLL) integrated circuit. The frequency multiplication factor, between the TCXO and VCO, can be varied, under microprocessor control, with a resolution of 2 parts in 10^{12}. A voltage-controlled attenuator at the 4.6 GHz output of the synthesizer allows for precise microprocessor control of the microwave amplitude applied to the physics package.

D. *Control Electronics*

The MAC control electronics are relatively simple, compared to conventional atomic clocks. In order to minimize component count, and thereby size and power consumption, many of the analog functions of traditional atomic clock architecture are implemented algorithmically in the MAC firmware. In addition to the physics package, the system consists principally of a microprocessor, multiple channels of analog input (ADC) and output (DAC), and the microwave synthesizer. The MAC operates from a single external 3.3 V supply, with internal regulators providing secondary regulation to 3.0 V and 2.8 V for the analog signal chain and the microwave synthesizer, respectively.

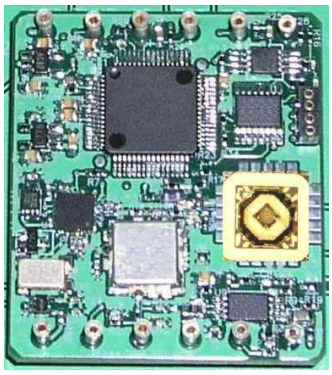

Figure 5. MAC Electronics

Figure 5 is a photograph of the complete MAC electronics. The physics package, with the vacuum lid removed, is on the right.

E. *Firmware*

Much of the complexity of the MAC control systems are implemented in firmware. Figure 6 shows a block diagram of the servo systems

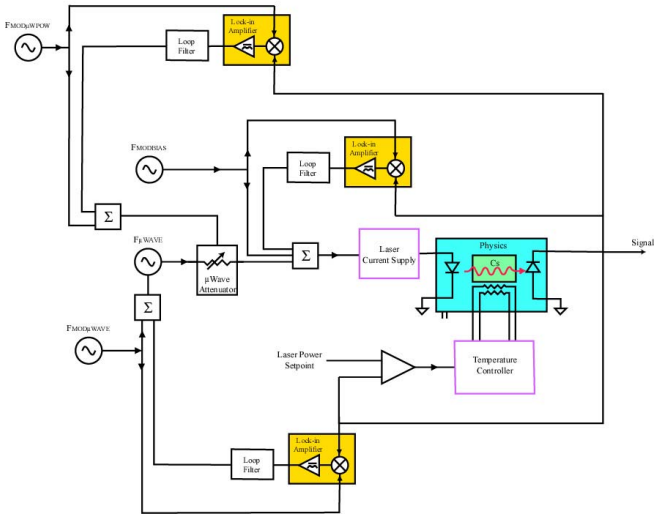

Figure 6. Block diagram of the MAC servos

Multiple servos are implemented in the firmware in order to simultaneously stabilize the temperature of the physics package, the laser bias current, the microwave power, and, of course, the clock frequency. Insofar as possible, these controls are servoed to measurements of atomic properties within the physics package. This approach stabilizes the characteristics of the CPT resonance and thus the clock frequency against long-term drift and environmental perturbations. Because there is only a single signal emerging from the physics package the multiple servos are operated at different frequencies (frequency division multiplexing) and/or at different times (time division multiplexing). The multiple phase-synchronous detectors (in yellow in Figure 6) are implemented entirely in firmware.

Upon initial start-up the firmware is responsible for initial optimization of the physics package temperature and microwave power and acquisition of the optical and microwave resonances. The firmware also provides internal parameter monitoring and an RS232 telemetry interface which allows for external monitoring of internal MAC operating parameters and alarm status and for providing input of precise frequency adjustment (calibration).

F. Power Budget

The MAC power budget is summarized in TABLE I.

TABLE I. MAC POWER BUDGET

System	Component	Power
Signal Processing	MicroController	20 mW
	16-Bit DACs	13 mW
	Analog	8 mW
Physics	Heater Power	7 mW
	VCSEL Power	3 mW
	C-Field	1 mW
Microwave/RF	4.6 GHz VCO	32 mW
	PLL	20 mW
	10 MHz TCXO	7 mW
	Output Buffer	1 mW
Power Regulation & Passive Losses		13 mW
Total		125 mW

III. MAC PERFORMANCE

In total, 15 MACs have been built and tested, including two engineering units and 13 pre-production units. The first engineering unit, SN084, has been extensively characterized while the second, SN087, was used as a testbed for hardware and firmware development. The subsequent 13 units, with serial numbers of the form SN3*xx*, were subjected to standard acceptance tests prior to delivery to proof-of-concept applications. Of these, three consecutive units, SN320-322, failed prematurely due to VCSEL failure. These three VCSELs were part of the same lot of four and thus we believe that these may have suffered latent damage due to electrostatic discharge (ESD) in process or handling.

A. Short-Term Stability

Compared to the optimal laboratory-scale electronics used to independently measure the physics package performance, as in Figure 3, some compromise in performance is expected with the low-power MAC electronics. In particular, the short-term stability of the MAC is degraded by noise on the VCSEL bias current and by phase noise on the microwave synthesizer.

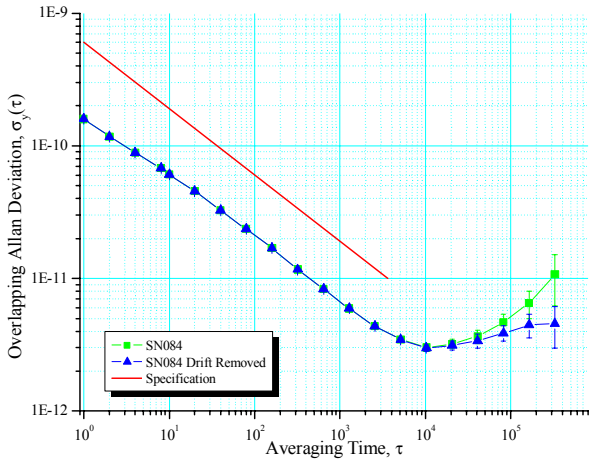

Figure 7: MAC SN084 Stability

Figure 7 shows the Allan deviation of MAC SN084 for a 3-week data period. SN084 is unique among the prototypes in that it has been operated for nearly 200 days and, as such, the frequency drift rate is relatively low ($<1\times10^{-11}$/day). The plot shows the specification (in red) along with the measured instability with and without the linear drift removed (in blue and green, respectively).

The short-term stability performance of SN084 is $\sigma_y(\tau)\approx1.5\times10^{-10}\tau^{-1/2}$, which is typical for all of the units built and tested to date.

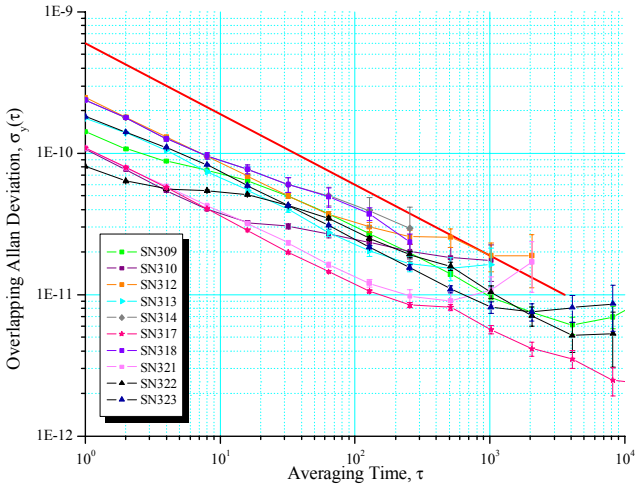

Figure 8. Collected STS data for 10 MACs

Figure 8 shows the stability data for 10 pre-production prototype MACs. All units exhibit $\sigma_y(\tau)<3\times10^{-10}\tau^{-1/2}$ out to averaging intervals of $\tau > 100$s. Because the phase data was collected shortly after assembly, linear drift was removed from the frequency data prior to the calculation of Allan deviation. Nonetheless, the long-term stability of the deliverable units diverges from ideal behavior at longer averaging times, principally due to early non-linear aging effects.

B. *Long-Term Drift*

The long-term frequency behavior of the engineering unit, SN084, has been monitored for ≈200 days. The measured frequency is shown below in Figure 9.

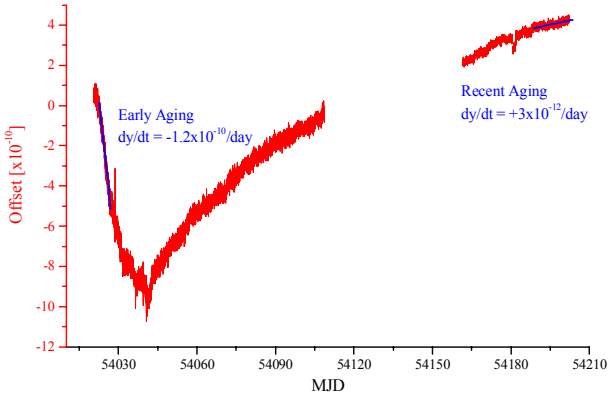

Figure 9. Long-term aging of SN084

The data of Figure 9 is "pieced together" from several data sets, including several unintentional power outages and a 45-day interruption during which the unit was removed from aging in order to update the electronics and firmware to the latest revision. Arbitrary frequency offsets were applied at Modified Julian Date (MJD) 54161 and MJD 54180 in order to realign the aging data.

The shape of the aging curve for SN084 appears to be typical for most of the MACs we have evaluated, though we do not have so long a data record for any other than SN084. Initially, the aging is fairly large (≈1.2×10^{-10}/day) and negative. Following approximately two weeks of negative aging, the aging changes sign and begins a cycle of exponentially-decaying positive aging. Towards the end of the data record, following 200 days of operation, the aging rate has reduced to ≈+3×10^{-12}/day (≈1×10^{-10}/month).

C. *Retrace*

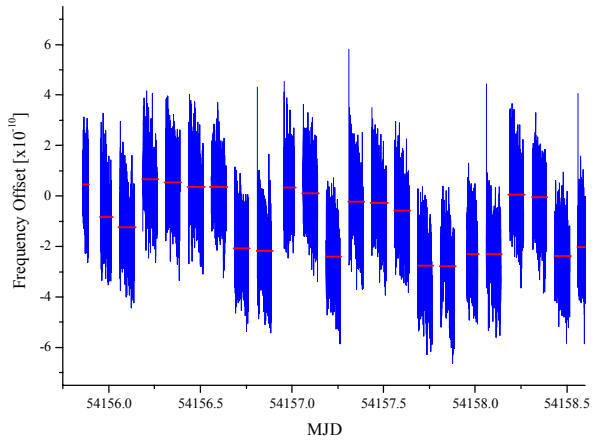

Figure 10. SN312 Retrace data

Retrace is defined to be the frequency error due to power-cycling the unit. In our laboratory, we measure retrace by periodically powering the unit from a household security timer while monitoring the frequency output.

Figure 10 shows a typical retrace measurement, during which MAC SN312 was cycled with a 2-hour on/1-hour off duty cycle. The blue trace is measured data and the red lines indicate the mean value of the frequency offset in each measurement interval. The frequency measurements are histogrammed in Figure 11, below.

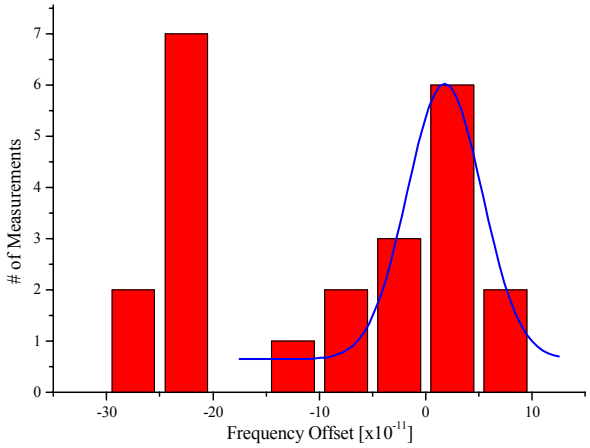

Figure 11. Histogram of Retrace values from Figure 10

It is clear from the data of Figure 10 and Figure 11 that the retrace behavior is bimodal. This reflects a shortcoming of the current MAC implementation. Including both retrace modes, the retrace (FWHM) is about $\Delta y=2\text{-}3\times10^{-10}$, whereas the retrace within a single mode (shown in blue) is only $\Delta y=7\times10^{-11}$. To varying extents, this behavior is typical of all 10 of the prototype MACs. In each case, the retrace of either mode is $\Delta y<1\times10^{-10}$, while the splitting between the modes is typically $\Delta y\approx1\times10^{-10}$ (as in SN312 shown above). In the worst case the modes are separated by $\Delta y\approx1\times10^{-9}$.

We suspect that the bimodal retrace behavior is the result of the VCSEL starting up randomly in either the x or y linear polarization state. In typical VCSELs (including ours), there is no strong anisotropy to select one linear polarization state over the orthogonal state. We have historically relied on a small amount of crystal strain, due to the fabrication or packaging processes, to break the symmetry and preferentially select a single operating polarization [11]. Modifications in our fabrication and/or packaging procedures have possibly reduced the amount of strain experienced by our VCSELs, causing less polarization discrimination. One potential long-term solution would be to fabricate VCSELs using shallow surface gratings to provide stronger polarization discrimination [12]. In the meantime, the cause and potential cures for the bimodal retrace remain under investigation.

D. *Performance over Temperature*

In real world applications, the MACs may be subjected to temperature variations of +/- 10°C and most require

qualification over a range of ΔT=0-50°C, or wider. In extreme temperature applications, the key parameters are power consumption and frequency change with temperature.

Because of the extraordinary thermal isolation of the physics package, the power consumption of the MAC is relatively insensitive to ambient temperature, compared to conventional atomic clocks. At lower operating temperatures, the physics package requires slightly more heater power (roughly 1 mW/7°C) but other components, such as the microprocessor, run more efficiently. The upper temperature limit is determined by the requirement to temperature-stabilize the physics package at ≈85°C. Even with the heaters turned off, the VCSEL dissipates ≈2mW, which limits the upper operating ambient to T≈70°C.

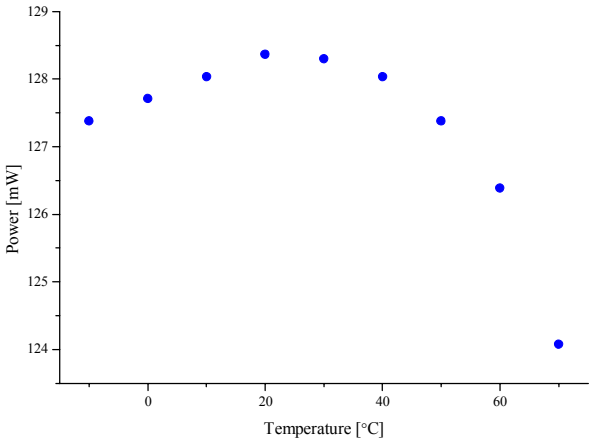

Figure 12. MAC Power Consumption vs. Ambient Temperature

Figure 12 shows the MAC power consumption as a function of ambient temperature. It is not surprising that the power consumption decreases by several milliWatts at elevated ambient (roughly 1 mW/7°C) from 40-70°C. It is surprising, though, that the power continues to drop at lower temperatures, indicating that the power savings of cooling the other electronic components offsets the increased heater power required by the physics package. In general, the power consumption changes by only 1-2%, from the nominal 125 mW, over the nominal operating range of 0-50°C.

The frequency change of the MAC over temperature is caused by several different and interacting sources, which affect the frequency of the cesium CPT resonance. The principal sources of CPT temperature coefficient are changes in the buffer gas and the laser spectrum which impact the collisional shift and AC Stark shift, respectively. In order to reduce the effects of the buffer gas collisions, the resonance cell is filled with a mixture of two buffer gases, Argon and Nitrogen, which produce oppositely signed shifts of the resonance line (-191 Hz/Torr and +924 Hz/Torr, respectively) [13]. Spectral variations are minimized, insofar as possible, by the servos, which stabilize the DC power of the VCSEL and optimize the microwave modulation amplitude. Nonetheless, there remains some temperature coefficient in the MAC, due to second-order buffer gas effects, spectral changes due to thermal gradients in the physics package, which change the DC bias point of the VCSEL, and other electronic effects, such as variation of the magnetic bias field circuit.

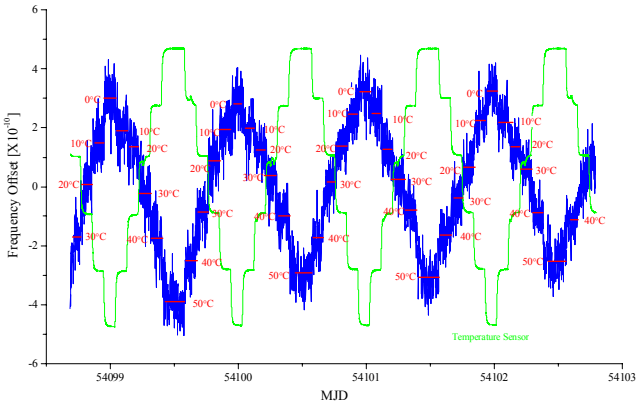

Figure 13. Uncompensated MAC temperature performance

Figure 13 shows the frequency offset of MAC SN310 (in blue) as the temperature is cycled from 0-50-0°C, in 10° steps, with a two-hour dwell at each temperature. Also shown is the temperature measured by the MAC internal temperature sensor (in green) and, in red, the average frequency offset in each measurement. Over the measurement range of 0-50°C, the MAC exhibits an approximately linear variation of $\Delta y/\Delta T \approx 8 \times 10^{-10}/50°C$.

The reproducible and nearly linear temperature response of Figure 13, along with the high correlation to the internal temperature sensor reading provides a mechanism for digital temperature compensation. The temperature coefficient of each unit is individually calibrated over temperature with respect to the internal temperature sensor measurement. In normal operation, the temperature sensor is continuously monitored and a small correction is applied to the microwave synthesizer.

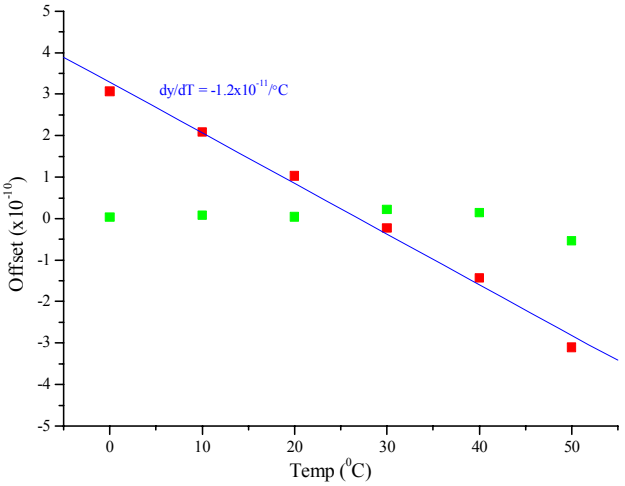

Figure 14. MAC Frequency Offset vs. Temperature with (green) and without (red) active compensation

Figure 14 shows the improvement in temperature performance resulting from digital compensation. The red points are the average values extracted from the measurement of Figure 8, along with a (blue) linear fit. The green points are extracted from a similar measurement on the same unit with the active compensation enabled. With compensation enabled, the temperature coefficient is no longer linear and has been reduced by approximately one order of magnitude to $\Delta y/\Delta T \approx 4x10^{-11}/50°C$.

In order for the compensation to be effective, not only must the measured (uncompensated) frequency be highly correlated with the reading from the onboard temperature sensor but, in addition, the correlation must be reproducible over many cycles, power-on retrace, and independent of whether the temperature is ramping up or down.

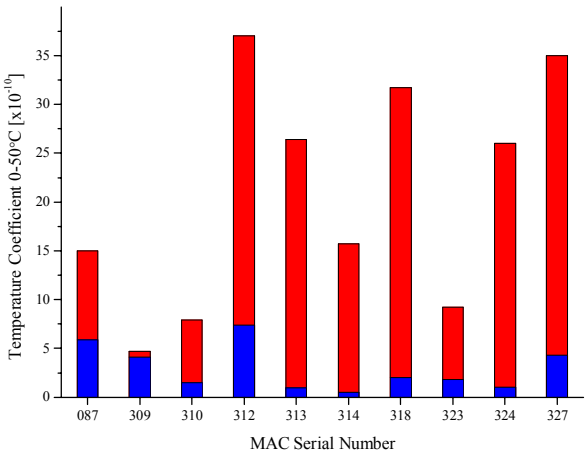

Figure 15. 0-50°C Temperature Coefficient of 10 MACs with compensation enabled (blue) and disabled (red)

Figure 15 shows the collected 0-50°C temperature coefficient for 10 of the MACs, without compensation (red) and with compensation enabled (blue). Uncompensated, most behave similarly to Figure 13, with temperature-driven frequency errors in the range of $\Delta y/\Delta T \approx 1\text{-}4x10^{-9}/50°C$. As Figure 15 shows, the compensation works fairly well for most units, reducing the temperature coefficient to $\Delta y/\Delta T < 5x10^{-10}/50°C$. For several units, the correlation between the uncompensated frequency change and the onboard temperature sensor is relatively poor, so that the compensation provides little, if any improvement. One unit in particular, SN309, exhibits poor symmetry between up-going temperature changes and down-going temperature changes, perhaps reflecting a thermal discontinuity within the physics package. Nonetheless, the average temperature coefficient for the 10 units shown in Figure 15 is $\Delta y/\Delta T = 3x10^{-10}/50°C$.

IV. Conclusion

We have built and tested 10 prototype miniature atomic clocks, with volume ≈15 cm^3 and power consumption ≈125 mW. All 10 devices exhibit excellent short-term stability of $\sigma_y(\tau) < 3x10^{-10}\tau^{-1/2}$. Over a temperature range of 0-50°C, the power varies by <5 mW and the frequency offset changes by $\Delta y < 4x10^{-10}$. The frequency drift, based on long-term measurements of a single unit, is better than $1x10^{-10}$/month, after 200 days of operation. Most units exhibit a bimodal retrace behavior, which is attributed to nearly degenerate polarization modes of the VCSEL.

Acknowledgments

The authors wish to acknowledge the following team members for valuable technical, theoretical, and moral support: J. Deng, D. Emmons, P. Vlitas, and R.M. Garvey of Symmetricom, K.M. Geib, V.M. Montano, G.A. Keeler, and T.M. Bauer of Sandia National Laboratories, and J. McElroy of the Charles Stark Draper Laboratory.

References

[1] R. Lutwak, et. al., "The MAC - a Miniature Atomic Clock," *Proceedings of the 2005 International Frequency Control Symposium*, August 29-31, 2005, Vancouver, BC, pp. 752–757.

[2] R. Lutwak, D. Emmons, W. Riley, and R.M. Garvey, "The Chip-Scale Atomic Clock – Coherent Population Trapping vs. Conventional Interrogation", *Proceedings of the 34th Annual Precise Time and Time Interval (PTTI) Systems and Applications Meeting*, December 3-5, 2002, Reston, VA, pp. 539-550.

[3] J. Kitching, et. al, IEEE Trans. Instrum. Meas. **49,** 1313 (2000).

[4] N. Cyr, M. Têtu, and M. Breton, IEEE Trans. Instrum. Meas. **42,** 640 (1993).

[5] R. Lutwak, et. al., "The Chip-Scale Atomic Clock – Low-Power Physics Package", *Proceedings of the 36th Annual Precise Time and Time Interval (PTTI) Systems and Applications Meeting*, December 7-9, 2004, Washington, DC, pp. 339-354.

[6] M. Mescher, R. Lutwak, and M. Varghese, "An Ultra-Low_power Physics Package for a Chip-Scale Atomic Clock," *Transducers '05, IEEE International Conference on Solid-State Sensors and Actuators*, June 5-9, 2005, Seoul, KoreaS.

[7] L-A. Liew, et. al. "Microfabricated alkali atom vapor cells," *Applied Physics Letters*, **84**, p. 2694 (2004).

[8] D.K. Serkland, et. al. "VCSELs for Atomic Sensors," *Proceedings of the SPIE*. Vol. 6484, 2007.

[9] R. Lutwak, D. Emmons, W. Riley, and R.M. Garvey, "The Chip-Scale Atomic Clock – Coherent Population Trapping vs. Conventional Interrogation", *Proceedings of the 34th Annual Precise Time and Time Interval (PTTI) Systems and Applications Meeting*, December 3-5, 2002, Reston, VA, pp. 539-550.

[10] S. Knappe, J. Kitching, L. Hollberg, and R. Wynands, Appl. Phys. B **74**, 217 (2002)

[11] T. Mukaihara, F. Koyama, K. Iga, "Engineered polarization control of GaAs/AlGaAs surface-emitting lasers by anisotropic stress from elliptical etched substrate hole," IEEE Photon. Technol. Lett., vol. 5, pp. 133-135 (1993).

[12] P. Debernardi, J. M. Ostermann, M. Feneberg, C. Jalics, and R. Michalzik, "Reliable polarization control of VCSELs through monolithically integrated surface gratings: a comparative theoretical and experimental study," IEEE J. Sel. Top. Quant. Electron., vol. 11, pp. 107-116 (2005).

[13] F. Strumia, N. Beverini, A. Moretti, "Optimization of the Buffer Gas Mixture for Opticlaly Pumped Cs Frequency Standards," *Proceedings of the 30th Annual Symposium on Frequency Control*, June 2-4, 1976